AAC Journals.ASM.org

Radiologic Responses in Cynomolgus Macaques for Assessing Tuberculosis Chemotherapy Regimens

Philana Ling Lin,[a] Teresa Coleman,[b] Jonathan P. J. Carney,[b] Brian J. Lopresti,[b] Jaime Tomko,[c] Dan Fillmore,[c] Veronique Dartois,[d] Charles Scanga,[c,e] L. James Frye,[e] Christopher Janssen,[f] Edwin Klein,[f] Clifton E. Barry III,[g] JoAnne L. Flynn[c,e]

Department of Pediatrics, Children's Hospital of Pittsburgh of the University of Pittsburgh Medical Center, University of Pittsburgh School of Medicine, Pittsburgh, Pennsylvania, USA[a]; Department of Radiology, University of Pittsburgh Medical Center, Pittsburgh, Pennsylvania, USA[b]; Department of Microbiology and Molecular Genetics, University of Pittsburgh School of Medicine, Pittsburgh, Pennsylvania, USA[c]; Department of Medicine, University of Medicine and Dentistry of New Jersey, Newark, New Jersey, USA[d]; Center for Vaccine Research, University of Pittsburgh, Pittsburgh, Pennsylvania, USA[e]; Division of Laboratory Animal Research, University of Pittsburgh, Pittsburgh, Pennsylvania, USA[f]; Tuberculosis Research Section, National Institute of Allergy and Infectious Diseases, National Institutes of Health, Bethesda, Maryland, USA[g]

Trials to test new drugs currently in development against tuberculosis in humans are impractical. All animal models to prioritize new regimens are imperfect, but nonhuman primates (NHPs) infected with *Mycobacterium tuberculosis* develop active tuberculosis (TB) disease with a full spectrum of lesion types seen in humans. Serial 2-deoxy-2-[^{18}F]-fluoro-D-glucose (FDG) positron emission tomography (PET) with computed tomography (CT) imaging was performed on cynomolgus macaques during infection and chemotherapy with individual agents or the four-drug combination therapy most widely used globally. The size and metabolic activity of lung granulomas varied among animals and even within a single animal during development of disease. Individual granulomas within untreated animals had highly local and independent outcomes, some progressing in size and FDG uptake, while others waned, illustrating the highly dynamic nature of active TB. At necropsy, even untreated animals were found to have a proportion of sterile lesions consistent with the dynamics of this infection. A more marked reduction in overall metabolic activity in the lungs (decreased FDG uptake) was associated with effective treatment. A reduction in the size of individual lesions correlated with a lower bacterial burden at necropsy. Isoniazid treatment was associated with a transient increase in metabolic activity in individual lesions, whereas a net reduction occurred in most lesions from rifampin-treated animals. Quadruple-drug therapy resulted in the highest decrease in FDG uptake. The findings of PET-CT imaging may provide an important early correlate of the efficacy of novel combinations of new drugs that can be directly translated to human clinical trials.

Successful treatment of tuberculosis (TB) disease requires a minimum of 6 months of therapy with multiple drugs. The mechanisms behind the slow response of TB to treatment are not well understood, and markers currently used in clinical trials (e.g., sputum conversion, early bactericidal activity) do not accurately predict treatment success (1, 2). The lack of reliable surrogate markers of drug efficacy hampers efforts to develop new drugs, shorten the treatment time, and reduce the disease burden. The events that occur in the lungs and other tissues to eliminate *Mycobacterium tuberculosis* during drug treatment are poorly understood, especially at the lesional level. There is evidence that specific lesion types, particularly cavities, are associated with poor treatment outcomes in patients (3), but for the many pathologies present in TB patients, we currently have little understanding of the kinetics of resolution by different drugs (4, 5). Assessing which lesions respond most slowly and optimizing regimens to resolve them offer a rational route forward to shortening the duration of chemotherapy; this is the ultimate goal for developing new treatment models. Assessing response rates in animal models of disease is difficult because necropsy is often the only time point at which accurate sampling can occur (6). This does not allow a comparison of disease before and after drug treatment, nor does it facilitate an analysis of the kinetics of the response from different subpopulations of lesions.

Standard chest radiography provides little detail on the array of lesions in lungs and lymph nodes in *M. tuberculosis*-infected hosts. Modern imaging technologies provide potentially useful tools to serially assess the drug response of TB in humans and animals. The most widely used positron emission tomography (PET) radiotracer is 2-deoxy-2-[^{18}F]-fluoro-D-glucose (FDG), a glucose analog that is taken up and retained by metabolically active cells, such as cancerous or inflammatory cells (e.g., macrophages, neutrophils, lymphocytes) (7–9). Coregistration of PET images with computed tomography (CT) images facilitates improved anatomic localization of areas of elevated FDG uptake. Incidental identification of biopsy-proven TB lesions has been described both anecdotally and in small case series among patients undergoing FDG PET-CT imaging for other diagnostic purposes (10–13). More recently, small pilot studies have been conducted to determine whether this method might be feasible in humans undergoing TB treatment (14–16), although validation data are limited. PET-CT has also been used in experimental animal models (e.g., mice and rabbits) to identify tuberculous disease and monitor the treatment response (17–19).

The nonhuman primate (NHP) model of TB provides impor-

Received 15 February 2013 Returned for modification 19 April 2013
Accepted 13 June 2013
Published ahead of print 24 June 2013
Address correspondence to JoAnne L. Flynn, joanne@pitt.edu.
Supplemental material for this article may be found at http://dx.doi.org/10.1128/AAC.00277-13.

doi:10.1128/AAC.00277-13

tant advantages since animals develop all disease pathologies seen in humans and pharmacokinetics in NHPs can generally be extrapolated to or from those in humans using conventional body weight allometric scaling rules (20, 21). We demonstrate here that serial FDG PET-CT imaging of NHPs during the course of *M. tuberculosis* infection and drug treatment provides a structural and functional dynamic map of disease-specific lesions and that the findings of FDG PET-CT imaging mirror the overall findings at necropsy. Our goal was to determine whether overall metabolic and/or radiographic changes as well as specific changes within individual granulomas could be used as a surrogate marker for drug efficacy. Our results indicate that granulomas evolve and resolve independently within a single host, that individual lesions respond differently to different drugs, and that overall PET and CT signals can predict successful drug treatment, validated by bacterial burden. These data have the potential to enhance the interpretation of PET-CT scans of TB patients, and PET-CT imaging may be used as a tool in predicting drug response in clinical trials for new TB drugs.

MATERIALS AND METHODS

***M. tuberculosis* infection and drug treatment.** Healthy, adult (>4 years old) cynomolgus macaques (*Macaca fascicularis*; Valley Biosystems, Sacramento, CA) were infected with either a low (25 CFU) or an intermediate (200 to 400 CFU) dose of *M. tuberculosis* strain Erdman via bronchoscopic instillation and monitored as previously described (20, 22). After infection, serial analyses for clinical (i.e., clinical monitoring of weight, cough, activity), microbiologic (i.e., analysis of gastric aspirate and bronchoalveolar lavage fluid for *M. tuberculosis* growth), and inflammatory (i.e., the erythrocyte sedimentation rate) markers were conducted every 2 to 4 weeks to determine disease progression, as previously described (20, 22). Once active disease was established (on the basis of clinical deterioration, persistent positive *M. tuberculosis* growth, and increased inflammatory markers, as previously described [20]), animals were randomly assigned to either drug or control groups. Animals were treated for 8 to 12 weeks, and ingestion of at least 90% of the prescribed dose was documented for all animals. Doses of rifampin (RIF; 20 mg/kg of body weight/dose once a day [QD]), isoniazid (INH; 15 mg/kg/dose QD), pyrazinamide (50 mg/kg/dose QD), and ethambutol (55 mg/kg/dose QD) were based on previous pharmacokinetic data (6) or derived from human doses. All animals with *M. tuberculosis* infection were maintained in a biosafety level 3 facility. Protocols and procedures were approved by the University of Pittsburgh's Institution for Animal Care and Use Committee.

Necropsy procedures. An FDG PET-CT scan was performed on every animal several days prior to necropsy to measure disease progression, and individual granulomas were obtained for histological analysis and bacterial burden. At necropsy, lesions previously identified by PET-CT imaging and lesions not seen in the lung and mediastinal lymph nodes on imaging were harvested. The size of each granuloma was measured at necropsy and by prenecropsy scan. The number of bacilli per individual granuloma was determined using the numbers of CFU per gram of granuloma tissue (20) multiplied by the weight of the granuloma, based on a standard curve of weight for granulomas of various sizes. Samples from liver and spleen as well as grossly apparent extrapulmonary lesions (if present) were also obtained, as previously described (20). Lesions were portioned for histopathology and bacterial burden, as previously described (20).

PET-CT imaging and analysis. All PET-CT scans were performed in a biosafety level 3 imaging suite using a hybrid preclinical PET-CT system that includes a micro-PET Focus 220 preclinical PET scanner (Siemens Molecular Solutions, Knoxville, TN) and an 8-slice helical CT scanner (Neurologica Corp., Danvers, MA) (23). A standardized uptake value (SUV) ratio (SUVR) was developed to normalize the degree of SUV variability between scans. Prior to treatment, lung granulomas ($n = 5$ to 8) from each monkey were randomly chosen, and partial volume corrections were made to each measurement on the basis of size of each lesion. The same analyst measured the size and SUV for all animals in this study. Metabolic activity for consolidations was measured by use of the glycolytic index (volume · mean SUV) on the basis of the volume of lung involved. Whole-lung PET was calculated by estimating the degree of abnormal lung density, measured by Hounsfield units, compared to that at the baseline by CT.

RESULTS

Development of TB disease assessed by serial FDG PET-CT. On the basis of our previous experience, infection with a low dose of 25 CFU resulted in approximately half of the animals developing active TB (20). To increase the rate of active disease, macaques were infected with an intermediate dose (200 to 400 CFU) of *M. tuberculosis* strain Erdman and scanned serially at monthly intervals. FDG was used as a probe to track the evolution of lung granulomas and thoracic lymph nodes in macaques following infection. Imaging parameters such as lesion number, number of lobes involved, size (on the basis of CT), and overall metabolic activity (on the basis of FDG uptake and measured as SUVRs) were used to assess disease progression. All animals that were scanned during the first 4 weeks postinfection (p.i.) had one or more thoracic lymph nodes with markedly elevated FDG uptake, suggesting an early inflammatory response to infection. The lymph nodes showed some fluctuations in size and SUVR over several months of infection but did not change dramatically as the disease worsened. However, in some lymph nodes it was possible to discern necrotic effacement (see Fig. S1 in the supplemental material) or mineralization as disease progressed, which was confirmed upon necropsy.

Individual granulomas in the lungs could be detected on PET-CT scan at as early as 2 to 4 weeks p.i. (Fig. 1). The median number of granulomas at 4 weeks was 46 ± 21 (range, 13 to 97; $n = 14$ monkeys). Nodules that appeared in the first 8 weeks measured between 1 and 11 mm in diameter (median = 2.4 mm) by CT, and FDG showed avidity for 99% (SUVR > 1.0) with a median SUVR of 14 (range, 0.7 to 40; $n = 177$ total granulomas analyzed). By 20 weeks p.i., mineralization was observed in 32% of lung lesions (18 of 56 randomly selected lesions) on CT.

Consolidations represent large areas of disease in the lungs, often consisting of tuberculous pneumonia. From a histological perspective, tuberculous pneumonia may be seen either as a primarily infiltrative progression involving the direct local extension of granulomatous infiltrates between contiguous airways or as a process of coalescence of expanding, rapidly developing granuloma substructures. These histologic observations fit well with what was observed by PET-CT imaging in this study, in that consolidations could arise from single lesions that increase in size and from coalescence of lesions. These were observed by 4 weeks p.i. in ~30% of monkeys receiving the intermediate dose (see Fig. S1 in the supplemental material). Consolidations ultimately developed in the lung lobe that was the site of the initial instillation in 68% of animals infected with this higher dose. The size and FDG avidity varied widely among consolidations in different animals. In general, lung consolidations increased in size and SUVR as clinical disease worsened, suggesting that consolidations contributed substantially to the development of active TB. PET data for consolidations were analyzed differently than those for small individual granulomas due to their size; a glycolytic index (mean SUVR relative to the volume of tissue) was calculated. Consolidations on

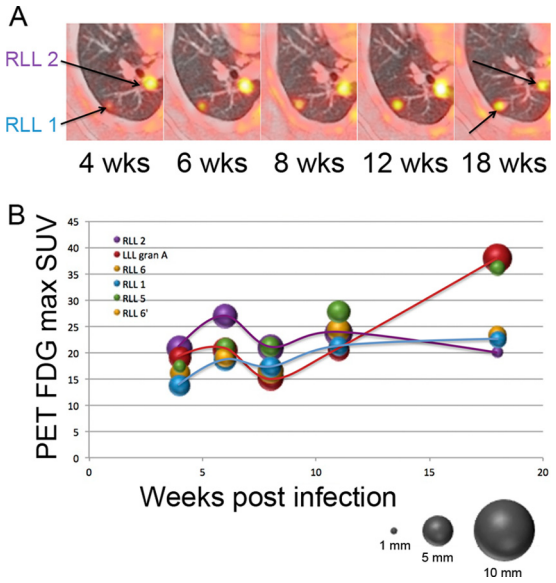

FIG 1 Lung granulomas are dynamic and independent. (A) Serial views of two granulomas in the right lower lobe (RLL) with independent changes in size and metabolic activity (yellow brightness) during early *M. tuberculosis* infection. (B) Granuloma size (based on the relative size of each sphere) and metabolic activity (SUV; *y* axis) are shown over time postinfection (*x* axis). Granulomas were from the same animal whose lung granulomas are depicted in panel A. Granuloma RLL 2 (purple) peaks in metabolic activity at 6 weeks postinfection, whereas granuloma RLL 1 (blue) peaks at 18 weeks postinfection. The granuloma in red increases dramatically at 18 weeks postinfection, unlike RLL 1 and RLL 2.

CT ranged from 0.84 to 83.97 cm^3 (median = 9.91 cm^3); the glycolytic index ranged from 2.72 to 592.38 mean SUVR · cm^3 (median = 48.77 mean SUVR · cm^3). Necrotic areas within individual granulomas and consolidations were identified by their characteristic pattern of a lack of central FDG uptake. Cavity formation developed in 15% (4 of 26) of animals in this study, with the majority (3 of 4) being associated with adjacent consolidation.

For this study, animals with active TB that developed from either intermediate-dose ($n = 18$) or low-dose ($n = 8$) infection were used and distributed equally among treatment groups (intermediate dose; 6 of 10 animals were controls, 5 of 7 animals were treated with isoniazid, 5 of 7 animals were treated with rifampin, and 2 animals were treated with isoniazid, rifampin, pyrazinamide, and ethambutol [HRZE]). Animals with low-dose infection were defined as having active TB on the basis of our published criteria (20). Likewise, animals infected with the intermediate dose in this study developed active disease that included at least one of the following: persistent positive *M. tuberculosis* growth in gastric aspirate or bronchoalveolar lavage fluid (17 of 18), elevated erythrocyte sedimentation rate (39%), cough (50%), and weight loss or anorexia (22%).

Lesions are independent and dynamic over time without treatment. Serial scanning allowed us to assess changes in individual lesions and lymph nodes over time, using characteristics that include lesion size and FDG avidity. To assess the general pattern of individual granulomas in a single monkey, a random sample of granulomas ($n = 5$ to 8) from each monkey was identified on CT and followed serially (an example of results for one monkey are shown in Fig. 1). After infection, both size and FDG avidity increased for a subset of these granulomas, and new granulomas occasionally appeared. However, not all granulomas in a single animal followed the same pattern of increased size and/or FDG avidity. Some granulomas were stable, while others actually decreased in size or the SUVR decreased, even within the same animal, during development of active TB. These data indicate that each individual lesion acts independently and that the overall trend of disease progression may depend on only a subset of lesions.

Bacterial load, histologic characteristics, and FDG avidity in granulomas from animals with active TB. Ten control monkeys that were followed by serial PET-CT scans were necropsied between 18 and 42 weeks postinfection as they developed disease. Using the PET-CT scan acquired immediately prior to necropsy as a guide, individually identified lung granulomas and lymph nodes were harvested and bisected for histology and bacterial enumeration. Granulomas from monkeys with active disease harbored a

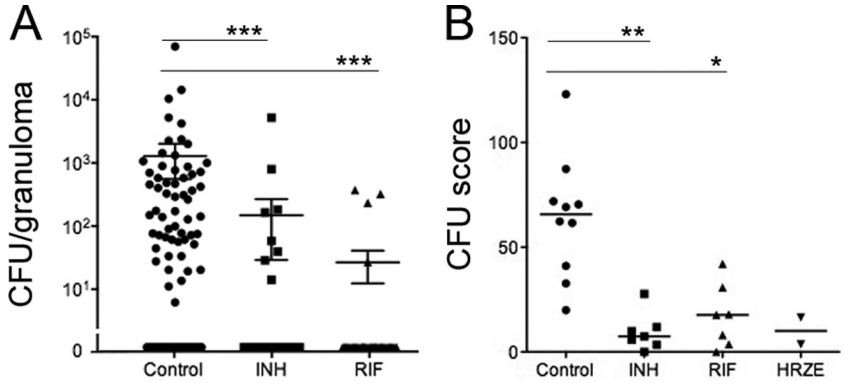

FIG 2 INH and RIF treatment reduces the bacterial burden within individual granulomas and in aggregate. (A) Granuloma bacterial burden (number of CFU per granuloma) was obtained at necropsy for control and treatment groups. Each dot is an individual granuloma. Sterile granulomas are depicted as 0 CFU and were found for 41 (of 99 total), 36 (of 43), and 33 (of 36) granulomas in the control, INH-treated, and RIF-treated animals, respectively. (B) The total bacterial burden was reduced in animals treated with INH alone and RIF alone compared to that in the controls. The CFU score reflects the overall bacterial burden within the entire animal. Each point represents the total bacterial burden of an animal. Too few data points were available for the HRZE-treated group for meaningful comparison. *P* values were determined by the Kruskall-Wallis test ($P < 0.001$) with *post hoc* analysis by Dunn's multiple-comparison test: *, $P \leq 0.05$; **, $P \leq 0.01$; ***, $P \leq 0.001$.

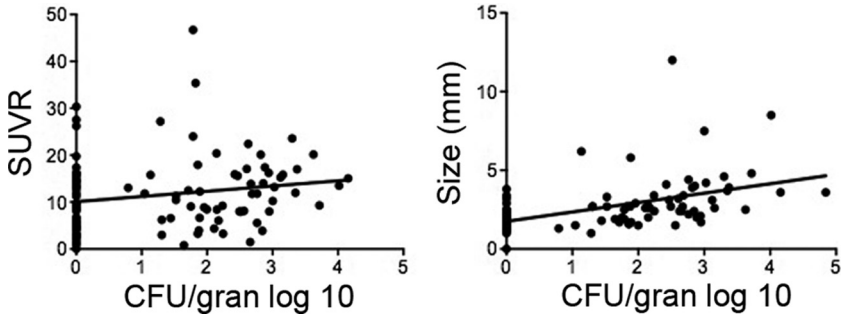

FIG 3 Lesional bacterial burden correlates with size but not SUVR in control animals with active TB. (Left) The bacterial burden within a granuloma (gran) did not specifically correlate to inflammation measured by FDG PET (SUVR) (linear regression, $R^2 = 0.03$, $P = 0.07$). (Right) A positive correlation between size and lesional bacterial burden was observed (linear regression, $R^2 = 0.244$, $P < 0.0001$).

large range of numbers of bacteria, up to 70,000 CFU per granuloma (Fig. 2A). We attempted to find an association between SUVR at the time of necropsy and bacterial burden for individual granulomas. In general, granulomas with high bacterial burdens did exhibit markedly elevated FDG uptake (Fig. 3, left). However, the reverse was not necessarily true: granulomas with high SUVRs could have a range of numbers of CFU per granuloma, and some granulomas with no culturable bacilli exhibited relatively high FDG uptake that overlapped with the observed SUVR values of lesions with culturable *M. tuberculosis*. Thus, there was no direct relationship between SUVR and exact bacterial numbers in granulomas identified in this study. However, the size of individual granulomas did correlate with bacterial numbers in control animals (Fig. 3, right). Granuloma characteristics (determined by histopathology) obtained at necropsy were also compared with FDG uptake and bacterial burden. While a broad range of granuloma types was observed, no direct relationship between SUVR and granuloma type was identified.

Thoracic lymph nodes are often culture positive in nonhuman primates with TB (20, 24). We identified lymph nodes based primarily on SUVR and then determined the bacterial load in each lymph node. In control monkeys, 83% of lymph nodes with FDG avidity had culturable bacilli (range, 0 to 41,000 CFU per lymph node).

FDG PET-CT can detect improvement of active TB upon drug treatment. We next investigated whether PET-CT could be used to assess the efficacy of drug treatment. The total FDG SUVR was calculated for the entire lung (excluding the thoracic lymph nodes) prior to and during drug treatment in each animal. Monkeys were randomized for treatment with either RIF ($n = 7$) or INH ($n = 7$) for 2 to 3 months. As controls, two monkeys were treated with HRZE. Overall PET-CT activity was reduced substantially by 2 months posttreatment among the RIF-, INH-, and HRZE-treated groups (Fig. 4). No reduction in overall PET activity was seen in control animals during the last 2 months prior to necropsy. The reduction in overall PET activity in the treatment groups was validated at necropsy by comparing the overall bacterial burden using our CFU scoring system (20). INH, RIF, and HRZE were effective in reducing the bacterial burden compared to no treatment (Fig. 2B).

Total FDG uptake is influenced by large areas of involvement with FDG avidity, such as consolidations (composed predominantly of tuberculous pneumonia). However, in human active TB, a range of granuloma types with different microenvironments and bacterial burdens are present (25, 26). We examined the effects of single-drug treatment on granuloma size and FDG uptake. Granulomas were randomly chosen (~5 to 6 per monkey, 7 monkeys per treatment group) for tracking during treatment with INH or RIF. There was a large range of SUVRs among granulomas prior to treatment, as in the controls. Rifampin treatment resulted in a significant reduction in the SUVR in individual granulomas at the end of treatment compared to pretreatment SUVRs (Fig. 5A). In

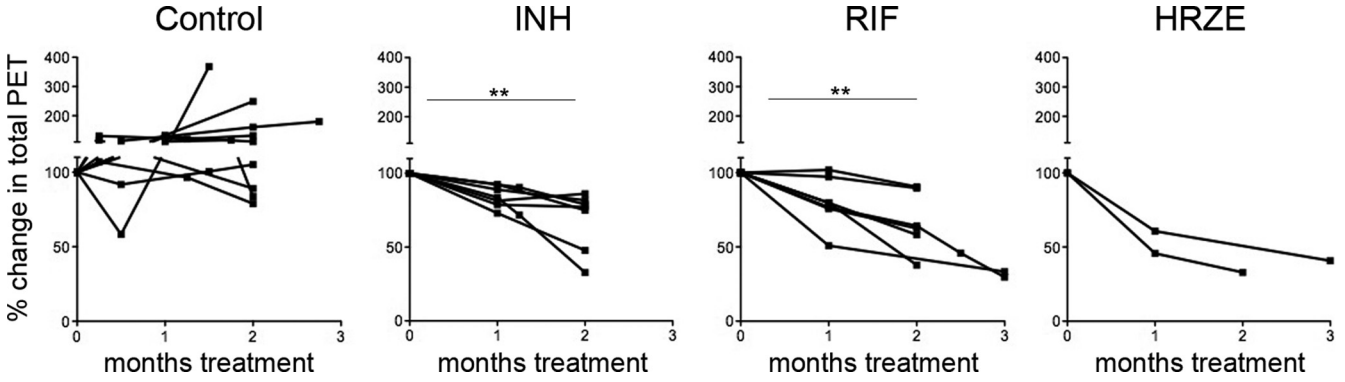

FIG 4 Treatment with INH, RIF, and HRZE results in reduced total PET activity from pretreatment levels. Total FDG uptake from the lungs was determined for each monkey before, during, and at the end of drug treatment. The *y* axis reflects the percent change of total SUV from pretreatment levels (100%). Each line represents an individual monkey. *P* values were determined by the Friedman test ($P < 0.001$) with *post hoc* analysis by Dunn's multiple-comparison test. **, $P < 0.01$. Too few data points were available for the HRZE-treated group for meaningful comparison.

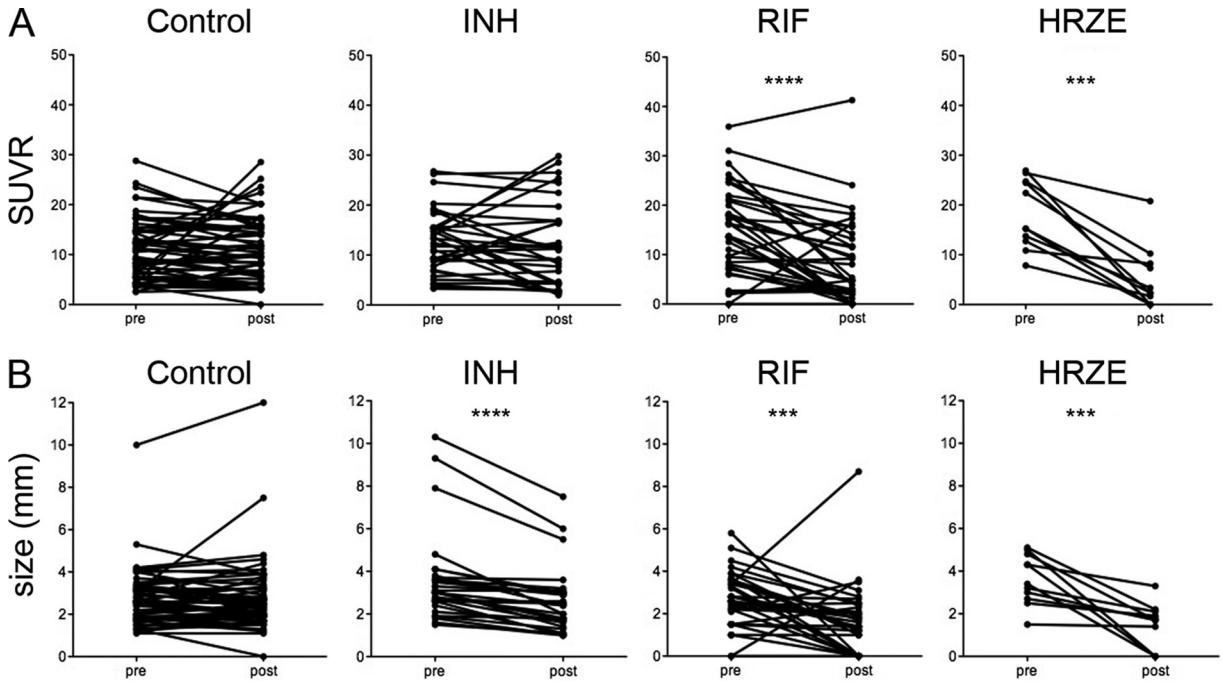

FIG 5 Serial measurements of granuloma SUV and size (mm) of monkeys immediately before (pre) and at the end (post) of drug treatment. (A) The metabolic activity of individual granulomas decreases with RIF and HRZE; (B) granuloma size decreases among animals treated with RIF alone, INH alone, and HRZE. *P* values were determined by the Wilcoxon matched-pairs sign-rank test: ***, $P \leq 0.001$; ****, $P \leq 0.0001$.

contrast, SUVRs in granulomas in INH-treated animals were more variable, with both increases and decreases in SUVRs being found. In the two HRZE-treated animals, there was a significant decrease in SUVRs in individual granulomas during treatment. In contrast, most of the granulomas in control (untreated) animals either showed no change in SUVR or increased over the 2 months prior to necropsy.

We also performed PET data analyses at the midpoint (after 1 month of treatment) (see Fig. S2 in the supplemental material). In both the RIF- and INH-treated groups, a number of the granulomas showed increased FDG uptake by 1 month posttreatment. In the RIF-treated group, the SUVRs of most of the granulomas then sharply decreased, while in the INH group the SUVR of many of the granulomas simply returned to the pretreatment SUVR. We interpret this increase in SUVR to be increased inflammation due to the killing of bacilli by the drug therapies, perhaps due to antigen release.

CT provides the opportunity to track changes in the size of individual granulomas during drug treatment. The majority of individual granulomas in control animals with active TB were relatively stable with respect to size over the 2 months prior to necropsy. In contrast, INH, RIF, and HRZE treatments resulted in significant reductions in granuloma size by the end of the treatment period (Fig. 5B). A significant reduction in granuloma size was observed at as early as 1 month after treatment in the INH and RIF treatment groups (see Fig. S2 in the supplemental material).

Consolidations represent large areas of disease in the lungs and are due to coalescing lesions or a single lesion that grows to a large size. Not all *M. tuberculosis*-infected macaques develop consolidations, although they are more prevalent following intermediate-dose infection than low-dose infection. By histopathology, consolidations are typically characterized as aggregates of caseous granulomas or tuberculous pneumonia and represent substantial disease. Treatment with either INH or RIF for 2 months was very effective at reducing both the size and the mean glycolytic index of consolidations (see Fig. S3 in the supplemental material). Control consolidations either progressed or were unchanged.

Lymph nodes. In both active disease and latent infection, at least one of the four to eight mediastinal lymph nodes is involved with either bacterial growth or granulomas; in some cases, lymph nodes can be completely effaced with granulomas at necropsy (20). In untreated control monkeys, in the 2 months prior to necropsy, FDG avidity was unchanged in most lymph nodes. However, in drug-treated animals, the lymph nodes were more dynamic in terms of FDG uptake, with the SUVR in many increasing over the course of treatment, particularly in the INH- or HRZE-treated group (see Fig. S4 in the supplemental material). Only a subset of lymph nodes in the drug-treated animals showed decreased FDG uptake. However, bacterial numbers in lymph nodes were low in drug-treated animals compared to the control animals, and many of the lymph nodes were sterilized following treatment with INH (75%), RIF (88%), or HRZE (100%) compared to the lymph nodes of the controls (41%).

Relationship of SUVRs and bacterial numbers in granulomas during short-term drug treatment. We compared SUVRs and bacterial numbers (numbers of CFU per granuloma) for several granulomas obtained at necropsy from each drug-treated animal. Most of the individual granulomas were sterilized by treatment with INH, RIF, and HRZE. There was not a simple correlation of SUVRs to bacterial numbers in individual granulomas following drug treatment. However, since granulomas in active TB can have a range of FDG avidities and bacterial numbers prior to the start of treatment, we reasoned that changes in SUVR (ΔSUVR) during treatment could correlate with bacterial number

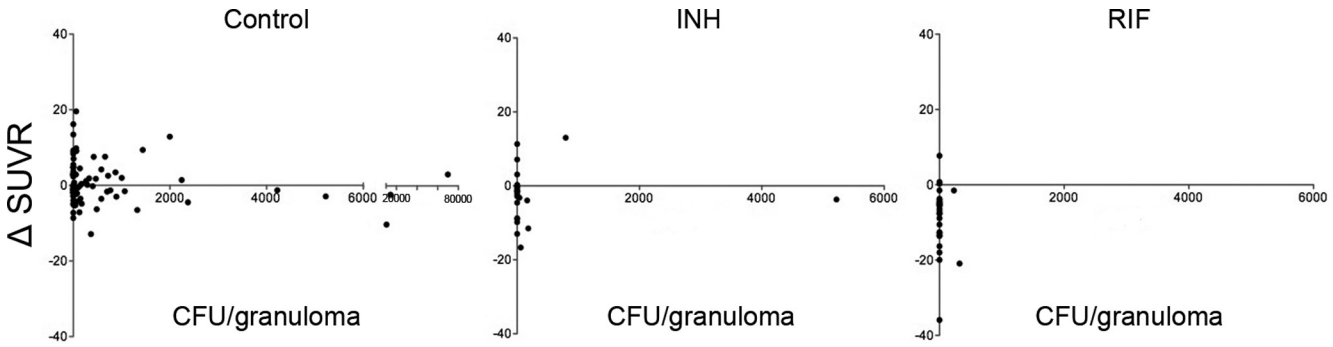

FIG 6 Reductions in SUVRs during INH or RIF treatment are observed with low bacterial numbers per granuloma. Each point represents a single granuloma from control ($n = 9$ animals), RIF-treated ($n = 7$ animals), and INH-treated ($n = 7$ animals) animals. Too few samples from the HRZE-treated group were available for meaningful analysis. Note that the *x* axis scale (CFU per granulomas) differs between the control and treatment groups due to high bacterial numbers in the control group.

at necropsy in individual granulomas. In control animals, there was no correlation between ΔSUVR and the number of CFU at necropsy (Fig. 6). The bacterial numbers were substantially lower in individual granulomas of drug-treated animals than in those of control animals (Fig. 2A). In control animals with active TB, 35% of individual granulomas were sterile ($n = 100$); this analysis necessarily excludes coalescing lesions and areas of pneumonia. In the RIF-treated animals, 26 of the 28 granulomas for which we measured the SUVR both pre- and posttreatment and obtained bacterial numbers were sterile (93%), and all but 2 of the sterile granulomas had a reduction in SUVR over the course of treatment. For INH, 17 of the 23 granulomas assessed for ΔSUVR and numbers of CFU at necropsy were sterile (74%), and of these, only 6 showed a reduction in SUVR over the treatment period. Of the 6 granulomas that still had culturable bacilli, 5 had reduced SUVRs. Thus, reductions in SUVR did correlate with enhanced clearance of bacteria in granulomas for RIF, but this was less obvious for INH at 2 months of treatment (Fig. 6).

Changes in the size of individual granulomas were also compared to bacterial numbers at necropsy. In control animals, the majority of granulomas with culturable bacilli, particularly those with more than 2,000 CFU per granuloma, demonstrated an increase in size over the 2 months prior to necropsy. In RIF- and INH-treated animals, the majority of the granulomas that had few or no culturable bacilli also had a decrease in size over the course of treatment (see Fig. S5 in the supplemental material).

The histopathological characteristics of granulomas that were followed serially by scan were analyzed. In our experience, fibrotic granulomas or those with interstitial fibrosis are associated with successful drug treatment, while posttreatment the remaining bacilli are primarily in nonresolved caseous granulomas (20). All fibrotic granulomas from the RIF and INH treatment groups were associated with a decreased ΔSUVR. Interstitial fibrosis was associated with a decreasing SUVR in all RIF-treated granulomas and most (67%) INH-treated granulomas. Thus, granulomas that were associated with healing were most prominent in the INH- and RIF-treated animals and were also more likely to have decreased FDG uptake in response to treatment.

DISCUSSION

Assessing the efficacy of anti-TB drugs in animal models is essential for identifying new therapeutics against this disease. Most drugs are tested in mice, and the results do not always translate to humans (27–29). However, testing drugs in nonhuman primates with tuberculosis, a model that closely mimics both the infection outcomes and pathology of human tuberculosis, can be challenging. Severity of disease is variable in macaques, just as in humans, and this makes it difficult to perform cross-sectional studies at different posttreatment intervals using distinct groups of animals. However, the advantage of animal models is that single-drug therapies can be performed and tissue data can be obtained at necropsy.

PET-CT has the potential to be an important tool for quickly assessing the efficacy of drugs against active TB; specifically, the most useful readout will likely be a combination of changes in size and SUV in individual lesions as well as overall. This technology can be used in human clinical trials of drugs in certain situations and should provide a more rapid assessment of drug efficacy. In this study, we used a higher dose of infection to obtain a higher percentage of animals with active TB disease. Using 200 to 400 CFU, virtually all animals developed active disease. With the PET-CT technology available to us, we were able to detect granulomas within the lungs as early as 3 weeks postinfection and granulomas that were as small as 1 mm in diameter. A striking finding was the dynamic nature of granulomas over time in individual animals, even in the absence of drug treatment. The majority of granulomas, following relatively high-dose infection, showed FDG avidity early postinfection. Over time, however, granulomas can change in size and FDG avidity, with some becoming bigger or smaller and some showing more or less FDG avidity. This reveals that granulomas have independent trajectories even without drug treatment. Surprisingly, sterile lesions were found in the untreated animals, yet these lesions were not always low in FDG avidity. Since FDG is incorporated into metabolically active cells, we interpret the sterile lesions showing FDG avidity to be those in which the immune response was sufficiently activated to kill the bacilli completely at some point prior to necropsy. In contrast to FDG avidity (SUVR), the size of the granuloma did correlate with bacterial numbers. In the rabbit model, there was a closer correlation of both SUVR and size with bacterial numbers, but the complexity of disease and granuloma types is less in rabbits (or mice), and rabbits have a relative paucity of sterile granulomas. This may have contributed to the differences with the NHP model seen here.

There are several ways to interpret the PET scan data from the

treated animals. When overall FDG uptake in the lungs was tracked, treatment with INH, RIF, or HRZE for 2 months led to substantial reductions in FDG uptake. Thus, examining the overall PET signal provides an assessment of drug efficacy within 2 months of treatment. Changes in the overall PET signal are primarily attributed to consolidated lung lesions that contribute to substantial bacterial burdens and are seen in severe human cases.

One advantage of serial PET-CT scanning is the ability to track individual granulomas and consolidations during treatment. Less dramatic but still significant changes were noted among individual granulomas. However, these lesions cannot be ignored, as they harbor bacteria that could lead to relapse. Among the control animals, in the 2 months prior to necropsy (which corresponds to the period of treatment in the drug-treated groups), most granulomas were fairly stable in terms of either FDG uptake or size. A substantial reduction in granuloma-specific bacterial burden and size was observed in all 3 treatment groups, despite the fact that significant decreases in FDG uptake were observed only in the group treated with RIF alone and HRZE and not in the group treated with INH alone. The persistence of FDG uptake even though the lesions had reduced bacterial burdens could be explained by increased inflammation in the lesions during early INH treatment, perhaps due to release of mycobacterial antigens. Since RIF and INH kill mycobacteria by different mechanisms, it may be that INH treatment leads to release of more lipid and protein antigens, which can cause inflammation. An alternative explanation may be that bacteria or bacterial debris is more slowly cleared from lesions during INH treatment, resulting in extended inflammation in individual granulomas. RIF has previously been reported to have anti-inflammatory properties that could influence the dramatic decrease in the SUVR observed shortly after treatment (30, 31), although this has not been described in the TB literature. Comparing lesions for which we obtained both the numbers of CFU per granuloma and SUVRs (Fig. 6), it is clear that even sterilized lesions in INH-treated animals (i.e., 0 CFU) occasionally showed increased SUVRs, while nearly all sterilized lesions in RIF-treated animals had a decreased SUVR over the treatment period. Perhaps a longer imaging interval is necessary with INH treatment to see reductions in SUVRs for all granulomas. In our previous studies in a rabbit model, the increase in FDG avidity in INH-treated animals was not observed at 4 weeks of treatment. There was a significant decrease in the SUVR in individual lesions at as early as 1 week and also by 2 months of treatment (19). The macaque develops a variety of lesion types, and it may be that some granuloma types respond to INH more quickly than other lesion types and these lesion types are more prominent in rabbits. In a similar fashion, early (at 1 to 3 months) and transient increases in blood gamma interferon responses have been observed during treatment of both latent and active TB with regimens that include INH (32–35).

In contrast to consolidations and individual granulomas, thoracic lymph nodes were much more difficult to assess for changes in FDG uptake during treatment. In fact, many of the lymph nodes exhibited increased FDG uptake during treatment. This likely reflects activated immune cells that are killing bacilli, since a higher fraction of lymph nodes was sterilized with drug treatment. It is also possible that antigens released by dying bacteria in the lung are transported to the lymph nodes by dendritic cells and the increased inflammation is due to activation of immune cells, including T cells or phagocytic cells. A limitation of FDG as a PET probe is its inability to distinguish the type of cell that is metabolically active.

In summary, we demonstrate here that serial PET-CT using FDG as a probe allows tracking of overall disease, individual granulomas, and lymph nodes during *M. tuberculosis* infection and treatment in an animal model of disease that is remarkably similar to the disease in humans. Using PET-CT, one can identify the efficacy of a single drug or a multidrug regimen within 1 to 2 months of treatment. This methodology holds the possibility of identifying different types of lesions that are not successfully treated by individual drugs (which may lead to treatment failure) and provides an early readout of the efficacy of new drugs prior to testing in humans.

ACKNOWLEDGMENTS

We thank the tireless efforts of Mark Rodgers, Catherine Cochran, Carolyn Bigbee, Matthew Bigbee, and Chelsea Chedrick for laboratory and technical assistance; Jim Mountz for radiology expertise; and Paul Johnston and Melanie O'Malley for veterinary assistance.

These studies were supported by the Bill and Melinda Gates Foundation TB Drug Accelerator and (in part) by the Intramural Research Program of the NIAID, NIH.

REFERENCES

1. **Wallis RS, Perkins MD, Phillips M, Joloba M, Namale A, Johnson JL, Whalen CC, Teixeira L, Demchuk B, Dietze R, Mugerwa RD, Eisenach K, Ellner JJ.** 2000. Predicting the outcome of therapy for pulmonary tuberculosis. Am. J. Respir. Crit. Care Med. **161**(4 Pt 1):1076–1080.
2. **Horne DJ, Royce SE, Gooze L, Narita M, Hopewell PC, Nahid P, Steingart KR.** 2010. Sputum monitoring during tuberculosis treatment for predicting outcome: systematic review and meta-analysis. Lancet Infect. Dis. **10:**387–394.
3. **Hamilton CD, Stout JE, Goodman PC, Mosher A, Menzies R, Schluger NW, Khan A, Johnson JL, Vernon AN.** 2008. The value of end-of-treatment chest radiograph in predicting pulmonary tuberculosis relapse. Int. J. Tuberc. Lung Dis. **12:**1059–1064.
4. **Im JG, Itoh H, Shim YS, Lee JH, Ahn J, Han MC, Noma S.** 1993. Pulmonary tuberculosis: CT findings—early active disease and sequential change with antituberculous therapy. Radiology **186:**653–660.
5. **Jeong YJ, Lee KS.** 2008. Pulmonary tuberculosis: up-to-date imaging and management. AJR Am. J. Roentgenol. **191:**834–844.
6. **Lin PL, Dartois V, Johnston PJ, Janssen C, Via L, Goodwin MB, Klein E, Barry CE, III, Flynn JL.** 2012. Metronidazole prevents reactivation of latent Mycobacterium tuberculosis infection in macaques. Proc. Natl. Acad. Sci. U. S. A. **109:**14188–14193.
7. **de Prost N, Tucci MR, Melo MF.** 2010. Assessment of lung inflammation with ^{18}F-FDG PET during acute lung injury. AJR Am. J. Roentgenol. **195:**292–300.
8. **Defawe OD, Hustinx R, Defraigne JO, Limet R, Sakalihasan N.** 2005. Distribution of F-18 fluorodeoxyglucose (F-18 FDG) in abdominal aortic aneurysm: high accumulation in macrophages seen on PET imaging and immunohistology. Clin. Nucl. Med. **30:**340–341.
9. **Ishimori T, Saga T, Mamede M, Kobayashi H, Higashi T, Nakamoto Y, Sato N, Konishi J.** 2002. Increased (18)F-FDG uptake in a model of inflammation: concanavalin A-mediated lymphocyte activation. J. Nucl. Med. **43:**658–663.
10. **Alavi A, Gupta N, Alberini JL, Hickeson M, Adam LE, Bhargava P, Zhuang H.** 2002. Positron emission tomography imaging in nonmalignant thoracic disorders. Semin. Nucl. Med. **32:**293–321.
11. **Goo JM, Im JG, Do KH, Yeo JS, Seo JB, Kim HY, Chung JK.** 2000. Pulmonary tuberculoma evaluated by means of FDG PET: findings in 10 cases. Radiology **216:**117–121.
12. **Kim YK, Lee KS, Kim BT, Choi JY, Kim H, Kwon OJ, Shim YM, Yi CA, Kim HY, Chung MJ.** 2007. Mediastinal nodal staging of nonsmall cell lung cancer using integrated ^{18}F-FDG PET/CT in a tuberculosis-endemic country: diagnostic efficacy in 674 patients. Cancer **109:**1068–1077.
13. **Yago Y, Yukihiro M, Kuroki H, Katsuragawa Y, Kubota K.** 2005. Cold tuberculous abscess identified by FDG PET. Ann. Nucl. Med. **19:**515–518.

14. **Sathekge M, Maes A, Kgomo M, Stolt A, Van de Wiele C.** 2011. Use of ^{18}F-FDG PET to predict response to first-line tuberculostatics in HIV-associated tuberculosis. J. Nucl. Med. **52:**880–885.
15. **Tian G, Xiao Y, Chen B, Xia J, Guan H, Deng Q.** 2010. FDG PET/CT for therapeutic response monitoring in multi-site non-respiratory tuberculosis. Acta Radiol. **51:**1002–1006.
16. **Martinez V, Castilla-Lievre MA, Guillet-Caruba C, Grenier G, Fior R, Desarnaud S, Doucet-Populaire F, Boue F.** 2012. (18)F-FDG PET/CT in tuberculosis: an early non-invasive marker of therapeutic response. Int. J. Tuberc. Lung Dis. **16:**1180–1185.
17. **Davis SL, Nuermberger EL, Um PK, Vidal C, Jedynak B, Pomper MG, Bishai WR, Jain SK.** 2009. Noninvasive pulmonary [^{18}F]-2-fluoro-deoxy-D-glucose positron emission tomography correlates with bactericidal activity of tuberculosis drug treatment. Antimicrob. Agents Chemother. **53:**4879–4884.
18. **Herschman HR.** 2003. Micro-PET imaging and small animal models of disease. Curr. Opin. Immunol. **15:**378–384.
19. **Via LE, Schimel D, Weiner DM, Dartois V, Dayao E, Cai Y, Yoon YS, Dreher MR, Kastenmayer RJ, Laymon CM, Carney JE, Flynn JL, Herscovitch P, Barry CE, III.** 2012. Infection dynamics and response to chemotherapy in a rabbit model of tuberculosis using [(18)F]2-fluoro-deoxy-D-glucose positron emission tomography and computed tomography. Antimicrob. Agents Chemother. **56:**4391–4402.
20. **Lin PL, Rodgers M, Smith L, Bigbee M, Myers A, Bigbee C, Chiosea I, Capuano SV, Fuhrman C, Klein E, Flynn JL.** 2009. Quantitative comparison of active and latent tuberculosis in the cynomolgus macaque model. Infect. Immun. **77:**4631–4642.
21. **McLeay SC, Morrish GA, Kirkpatrick CM, Green BB.** 2012. The relationship between drug clearance and body size: systematic review and meta-analysis of the literature published from 2000 to 2007. Clin. Pharmacokinet. **51:**319–330.
22. **Capuano SV, III, Croix DA, Pawar S, Zinovik A, Myers A, Lin PL, Bissel S, Fuhrman C, Klein E, Flynn JL.** 2003. Experimental Mycobacterium tuberculosis infection of cynomolgus macaques closely resembles the various manifestations of human M. tuberculosis infection. Infect. Immun. **71:**5831–5844.
23. **Rumbolt Z, Huda W, All JW.** 2009. Review of portable CT with assessment of a dedicated head CT scanner. Am. J. Neuroradiol. **30:**1630–1636.
24. **Lin PL, Pawar S, Myers A, Pegu A, Fuhrman C, Reinhart TA, Capuano SV, Klein E, Flynn JL.** 2006. Early events in Mycobacterium tuberculosis infection in cynomolgus macaques. Infect. Immun. **74:**3790–3803.
25. **Canetti G.** 1955. The tubercle bacillus. Springer Publishing Co, Inc, New York, NY.
26. **Leong FJ, Eum SK, Via L, Barry CE, III.** 2011. Pathology of tuberculosis in human lung. *In* Leong FJ, Dartois V, Dick T (ed), A color atlas of comparative pathology of pulmonary tuberculosis. CRC Press, Boca Raton, FL.
27. **Cynamon MH, Klemens SP, Sharpe CA, Chase S.** 1999. Activities of several novel oxazolidinones against Mycobacterium tuberculosis in a murine model. Antimicrob. Agents Chemother. **43:**1189–1191.
28. **Lee M, Lee J, Carroll MW, Choi H, Min S, Song T, Via LE, Goldfeder LC, Kang E, Jin B, Park H, Kwak H, Kim H, Jeon HS, Jeong I, Joh JS, Chen RY, Olivier KN, Shaw PA, Follmann D, Song SD, Lee JK, Lee D, Kim CT, Dartois V, Park SK, Cho SN, Barry CE, III.** 2012. Linezolid for treatment of chronic extensively drug-resistant tuberculosis. N. Engl. J. Med. **367:**1508–1518.
29. **Williams KN, Stover CK, Zhu T, Tasneen R, Tyagi S, Grosset JH, Nuermberger E.** 2009. Promising antituberculosis activity of the oxazolidinone PNU-100480 relative to that of linezolid in a murine model. Antimicrob. Agents Chemother. **53:**1314–1319.
30. **An N, Song Y, Zhang X, Ci X, Li H, Cao Y, Zhang M, Cui J, Deng X.** 2008. Pretreatment of mice with rifampicin prolongs survival of endotoxic shock by modulating the levels of inflammatory cytokines. Immunopharmacol. Immunotoxicol. **30:**437–446.
31. **Nau R, Wellmer A, Soto A, Koch K, Schneider O, Schmidt H, Gerber J, Michel U, Bruck W.** 1999. Rifampin reduces early mortality in experimental Streptococcus pneumoniae meningitis. J. Infect. Dis. **179:**1557–1560.
32. **Lee SW, Lee SH, Yim JJ.** 2012. Serial interferon-gamma release assays after chemoprophylaxis in a tuberculosis outbreak cohort. Infection **40:**431–435.
33. **Dyrhol-Riise AM, Gran G, Wentzel-Larsen T, Blomberg B, Haanshuus CG, Morkve O.** 2010. Diagnosis and follow-up of treatment of latent tuberculosis; the utility of the QuantiFERON-TB Gold in-tube assay in outpatients from a tuberculosis low-endemic country. BMC Infect. Dis. **10:**57. doi:10.1186/1471-2334-10-57.
34. **Wilkinson KA, Kon OM, Newton SM, Meintjes G, Davidson RN, Pasvol G, Wilkinson RJ.** 2006. Effect of treatment of latent tuberculosis infection on the T cell response to Mycobacterium tuberculosis antigens. J. Infect. Dis. **193:**354–359.
35. **Lee SW, Lee CT, Yim JJ.** 2010. Serial interferon-gamma release assays during treatment of active tuberculosis in young adults. BMC Infect. Dis. **10:**300. doi:10.1186/1471-2334-10-300.